01 Mar 2014

Seismic Anisotropy and Mantle Flow beneath the Northern Great Plains of North America

Bin B. Yang

Stephen S. Gao
Missouri University of Science and Technology, sgao@mst.edu

Kelly H. Liu
Missouri University of Science and Technology, liukh@mst.edu

Ahmed A. Elsheikh

et. al. For a complete list of authors, see https://scholarsmine.mst.edu/geosci_geo_peteng_facwork/416

Recommended Citation

B. B. Yang et al., "Seismic Anisotropy and Mantle Flow beneath the Northern Great Plains of North America," *Journal of Geophysical Research: Solid Earth*, vol. 119, no. 3, pp. 1971-1985, John Wiley & Sons Ltd, Mar 2014.
The definitive version is available at https://doi.org/10.1002/2013JB010561

AGU PUBLICATIONS

JGR

Journal of Geophysical Research: Solid Earth

RESEARCH ARTICLE

10.1002/2013JB010561

Key Points:
- We measured over 4000 pairs of splitting parameters
- We proposed a model involving flow deflection
- Results have broader impacts

Supporting Information:
- Table S1
- Table S2

Correspondence to:
S. S. Gao,
sgao@mst.edu

Citation:
Yang, B. B., S. S. Gao, K. H. Liu, A. A. Elsheikh, A. A. Lemnifi, H. A. Refayee, and Y. Yu (2014), Seismic anisotropy and mantle flow beneath the northern Great Plains of North America, *J. Geophys. Res. Solid Earth*, *119*, 1971–1985, doi:10.1002/2013JB010561.

Received 27 JUL 2013
Accepted 23 JAN 2014
Accepted article online 28 JAN 2014
Published online 19 MAR 2014

Seismic anisotropy and mantle flow beneath the northern Great Plains of North America

Bin B. Yang[1], Stephen S. Gao[1], Kelly H. Liu[1], Ahmed A. Elsheikh[1], Awad A. Lemnifi[1], Hesham A. Refayee[1], and Youqiang Yu[1]

[1]Geology and Geophysics Program, Missouri University of Science and Technology, Rolla, Missouri, USA

Abstract A diverse set of tectonic features and the recent availability of high-quality broadband seismic data from the USArray and other stations on the northern Great Plains of North America provide a distinct opportunity to test different anisotropy-forming mechanisms. A total of 4138 pairs of well-defined splitting parameters observed at 445 stations show systematic spatial variations of anisotropic characteristics. Azimuthally invariant fast orientations subparallel to the absolute plate motion (APM) direction are observed at most of the stations on the Superior Craton and the southern Yavapai province, indicating that a single layer of anisotropy with a horizontal axis of symmetry is sufficient to explain the anisotropic structure. For areas with simple anisotropy, the application of a procedure for estimating the depth of anisotropy using spatial coherency of splitting parameters results in a depth of 200–250 km, suggesting that the observed anisotropy mostly resides in the upper asthenosphere. In the vicinity of the northern boundary of the Yavapai province and the Wyoming Craton, the splitting parameters can be adequately explained by a two-horizontal layer model. The lower layer has an APM-parallel fast orientation, and the upper layer has a fast orientation that is mostly consistent with the regional strike of the boundary. Based on the splitting measurements and previous results from seismic tomography and geodynamic modeling, we propose a model involving deflecting of asthenosphere flow by the bottom of the lithosphere and channeling of flow by a zone of thinned lithosphere approximately along the northern boundary of the Yavapai province.

1. Introduction

Intensive geological and geophysical research over the past several decades has demonstrated that mechanical anisotropy is a pervasive characteristic of the Earth's crust and upper mantle. Measurements of the strength and orientation of seismic anisotropy from splitting of teleseismic *P*-to-*S* converted phases at the core-mantle boundary on the receiver side, such as *SKS*, *SKKS*, and *PKS* (hereinafter are collectively called *XKS*) have provided the geoscientific community with important information on the structure and deformation of the Earth's deep interior [*Silver*, 1996; *Savage*, 1999; *Fouch and Rondenay*, 2006; *Long and Silver*, 2009]. The splitting parameters, the fast orientation (ϕ) and the splitting time between the fast and slow split shear waves (δt), are measurements of the orientation and strength of the anisotropy, respectively, and have been increasingly used by a wide range of geoscientists to understand crustal and mantle structure and dynamics [*Silver and Holt*, 2002; *Maupin et al.*, 2005; *Becker et al.*, 2006; *Fouch and Rondenay*, 2006; *Marone and Romanowicz*, 2007; *Kreemer*, 2009; *Gao et al.*, 2010; *Yuan and Romanowicz*, 2010; *Conrad and Behn*, 2010; *Satsukawa et al.*, 2011; *Huang et al.*, 2011; *Li et al.*, 2011].

In spite of the numerous studies, the origin of the observed seismic anisotropy is still a topic of much debate. While the lattice preferred orientation (LPO) of the crystallographic axis of olivine is believed to be the main cause of anisotropy, whether the LPO mostly takes place in the lithosphere or the asthenosphere is still not certain [*Silver*, 1996; *Frederiksen et al.*, 2007]. In the lithosphere, most studies proposed that the LPO associated with past tectonic events was responsible for the observed anisotropy with a fast orientation parallel to the strike of the orogenic zones [*Silver*, 1996; *Fouch and Rondenay*, 2006], and in the asthenosphere, the LPO could result from simple shear originated from flow gradient [*Vinnik et al.*, 1992; *Bormann et al.*, 1996; *Tommasi et al.*, 1996]. Another possible mechanism that can form anisotropy in the mantle is preferably oriented magmatic dikes in the lithosphere [*Gao et al.*, 1997, 2010; *Kendall et al.*, 2005].

The northern Great Plains of North America (Figure 1) is well sampled by the USArray stations with outstanding data quality and has experienced various of deformational and magmatic events from the Precambrian

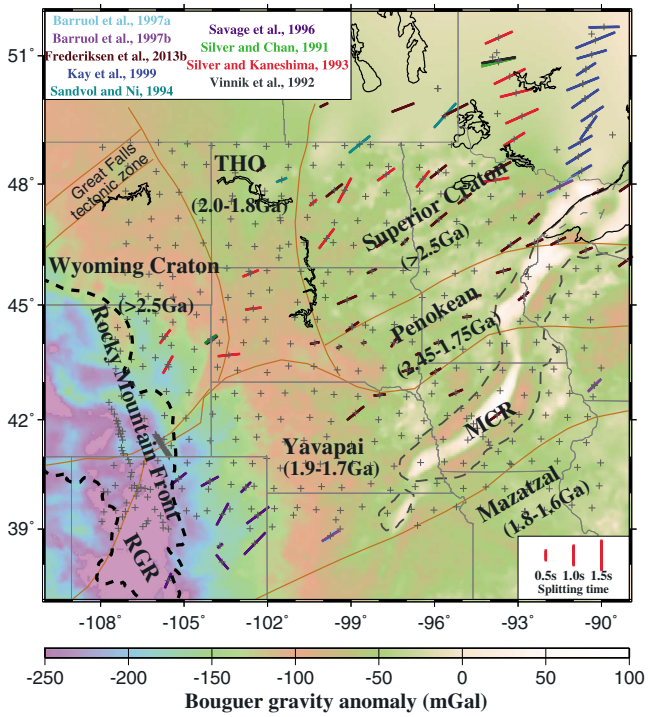

Figure 1. Bouguer gravity anomaly map of the study area showing seismic stations used in the study (pluses) and major tectonic provinces. The solid brown lines separate Precambrian basement terranes [*Hoffman*, 1988; *Zhao et al.*, 2002]. Also shown are previous shear wave splitting measurements in the study area [*Silver and Chan*, 1991; *Vinnik et al.*, 1992; *Silver and Kaneshima*, 1993; *Sandvol and Ni*, 1994; *Savage et al.*, 1996; *Barruol et al.*, 1997a, 1997b; *Kay et al.*, 1999; *Frederiksen et al.*, 2013b]. For a given study, the same color is used for the citation in the legend and the bars in the map. THO: Trans-Hudson orogeny; MCR: Midcontinent rift; RGR: Rio Grande rift.

to the Cenozoic [*Karlstrom and Bowring*, 1988; *Whitmeyer and Karlstrom*, 2007]. Major tectonic provinces include the Archean Superior Craton (>2.5 Ga), Penokean orogeny (2.45–1.75 Ga), Trans-Hudson orogeny (THO, 2.0–1.8 Ga), Wyoming Craton (>2.5 Ga), Yavapai province (1.9–1.7 Ga), Proterozoic Midcontinent rift (MCR, >1.1 Ga), and the Cenozoic Rio Grande rift [*Whitmeyer and Karlstrom*, 2007]. Precambrian accretion of Archean microcontinents formed most of the basement in the area [*Hoffman*, 1989; *Davidson*, 1995; *Holm*, 1999]. The Cenozoic widespread extension created a series of magmatic episodes and formed the Rio Grande rift [*Morgan et al.*, 1986; *Coward et al.*, 1987; *Baldridge et al.*, 1991; *Balch et al.*, 1997; *Mosher*, 1998; *Lawton and McMillan*, 1999; *McMillan et al.*, 2000].

Seismic body wave tomographic models suggested a high-velocity feature beneath the western Superior Craton, probably associated with elevated lithospheric anisotropy [*Grand and Helmberger*, 1984; *Frederiksen et al.*, 2013a, 2013b]. Beneath the Superior Craton, the thickness of the lithosphere varies between 200 and 250 km [*Darbyshire et al.*, 2007; *Darbyshire and Lebedev*, 2009]. A low-velocity channel-shaped feature was proposed toward the southeast through the southern extreme of the THO and Superior Craton into the Penokean orogeny [*Frederiksen et al.*, 2013a], approximately along the northern edge of the Yavapai province. Three possibilities, including a mantle plume, a failed branch of the MCR, and an older feature from the Superior accretion, were proposed for the origin of the channel [*Frederiksen et al.*, 2013a]. The thickness of the lithosphere beneath the Great Plains is about 200–250 km and reduces to about 125 km beneath the western U.S. orogenic zone [*van der Lee and Frederiksen*, 2005; *Darbyshire et al.*, 2007; *Bedle and van der Lee*, 2009; *Darbyshire and Lebedev*, 2009; *Yuan and Romanowicz*, 2010].

The vast majority of the previous shear wave splitting (SWS) investigations in the study area (Figure 1) assumed a single layer of anisotropy with a horizontal axis of symmetry. A study conducted by *Silver and Chan* [1991] involved two stations on the Superior Craton. Large splitting times (>1.7 s) and NE-E fast orientations were observed. A lithospheric deformation model was proposed to explain the obtained splitting parameters. The same stations were used by *Vinnik et al.* [1992] to suggest that there was a positive correlation between the absolute plate motion (APM) direction and the fast orientation of anisotropy. *Silver and*

Kaneshima [1993] found that the fast orientations displayed good geologic coherence in the western Superior Craton and the THO, and the delay times (0.40–1.75 s) showed systematic variations across the transition zone of the two areas. They concluded that Precambrian fossil fabrics preserved in the subcontinental lithosphere dominated the observed anisotropy. *Savage et al.* [1996] reported variable splitting parameters and implied a single-layer anisotropy structure across the Rocky Mountain Front. They proposed that the fast orientations were consistent within small geographic regions and that weak anisotropy with a horizontal symmetry axis was present beneath the study area. A model of asthenospheric flow converging on or diverging from the central uplifted region of the Rocky Mountain Front was postulated. *Barruol et al.* [1997a] suggested the existence of an asthenosphere flow channeled around the North American cratonic root. *Frederiksen et al.* [2007] proposed a lithospheric anisotropy and reported splitting parameters as ENE-WSW and 1.34 s at stations west of 86°W and E-W and 0.67 s on the eastern Superior Craton. *SKS* splitting measurements at 40 stations in the U.S. and five in Canada on the Superior Craton and surrounding areas were attributed to lithospheric fabrics (Figure 1) [*Frederiksen et al.*, 2013b].

Complex anisotropy was proposed by recent studies for portions of the study area. *Yuan and Romanowicz* [2010] used a three-layer anisotropy model beneath central North America to interpret the results of surface wave inversion. The top layer resides in the lithosphere and the fast orientation is mostly consistent with the geological trends, indicating ancient orogenic collisional activities. The middle layer, which is also in the lithosphere, has a N-S fast orientation, while the bottom layer, which is in the asthenosphere, is dominated by NE-SW fast orientations which are subparallel to the APM direction of the North American Plate. Beneath the southwestern edge of the North American continent, *Refayee et al.* [2013] suggested a single layer of anisotropy in the majority of the areas. They proposed that shearing between the partially coupled lithosphere and asthenosphere was the origin of the observed anisotropy, with small contributions from the lithosphere beneath areas with two-layer anisotropy. A model involving deflecting of asthenospheric flow along the western and southern edges of the North American continent was used to interpret the observed edge-parallel fast orientations and large splitting times.

The northern Great Plains is an ideal locale for distinguishing different anisotropy models (lithospheric, asthenospheric, or both) and for investigating the degree of coupling of lithosphere and asthenosphere, for the following reasons: (1) There are several major Precambrian tectonic provinces such as the Superior Craton, THO, Wyoming Craton, and the MCR with spatially varying lithospheric thickness and tectonic trends; (2) There is an excellent spatial coverage by the USArray stations from which numerous splitting parameters can be obtained; (3) A number of recent seismic tomographic [*Yuan and Romanowicz*, 2010; *Frederiksen et al.*, 2013a, 2013b] and geodynamic modeling studies [*Forte et al.*, 2007; *Conrad and Behn*, 2010] in the area provided additional constraints on anisotropy-forming mechanisms.

2. Data and Methods

The broadband seismic data used in the project were recorded by 388 stations of the USArray, 19 permanent and 38 portable stations from 1992 to 2012 within the area of 108°W–90°W and 39°N–51°N. We requested data from the IRIS (Incorporated Research Institutions for Seismology) DMC (Data Management Center) based on the criteria that the epicentral distance for *PKS*, *SKKS*, and *SKS* is 120°–180°, 95°–180°, and 84°–180°, respectively [*Gao and Liu*, 2009], and that the minimum magnitude is 5.6 for all the events with the focal depths less than 100 km. For deeper events, the corresponding magnitude is reduced by 0.1 in order to make better use of the sharper waveform.

Based on the method of minimizing energy on the corrected transverse component [*Silver and Chan*, 1991], *Liu* [2009] produced a set of robust procedures to obtain reliable SWS parameters. A band-pass filter with corner frequencies of 0.04–0.5 Hz was applied to the seismograms. An automatic data selection procedure was used to reject *XKS* waveforms with low signal-to-noise ratio on the original radial component [*Gao and Liu*, 2009; *Liu and Gao*, 2013]. Visual inspections were made to all the measurements, and manual adjustments were applied when necessary, on the start and end times of the *XKS* window, on the quality ranking determined automatically, and on the band-pass filtering frequencies [*Liu and Gao*, 2013]. A total of 445 stations (Figure 1) were found to have at least one quality A or B [*Liu et al.*, 2008] *XKS* measurement. The number of events used in the study is 492 (Figure 2).

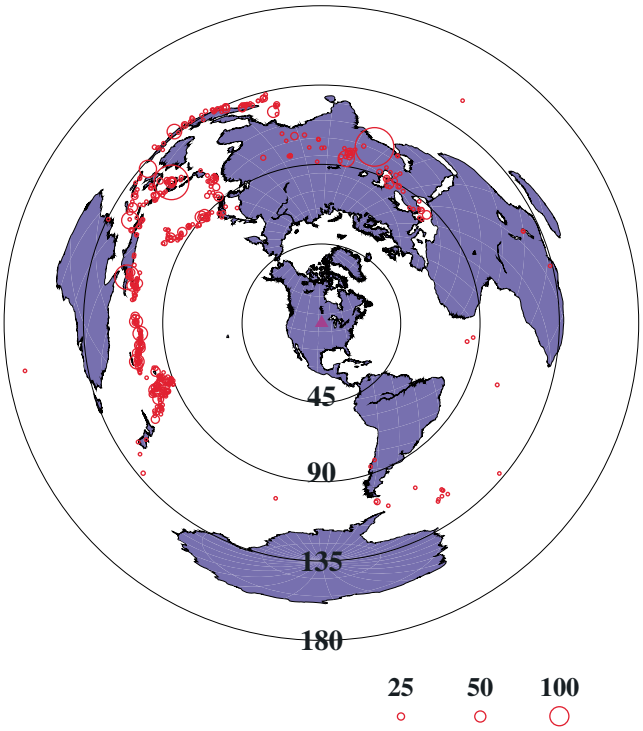

Figure 2. Azimuthal equidistant projection map showing earthquakes used in the study (open dots). The radius of the dots is proportional to the number of resulting well-defined splitting measurements from the events.

3. Results

A total of 4138 pairs of well-defined (quality A and B, see *Liu et al.* [2008] for ranking criteria) splitting parameters are obtained, including 447 for *PKS*, 749 for *SKKS*, and 2942 for *SKS* measurements (Figure 3; See also Tables S1 and S2 in the supporting information). The mean value of the splitting times (Figure 4) over all the measurements is 0.98±0.32 s which is almost the same as the global average of 1.0 s for continents [*Silver*, 1996] and corresponds to a 110±30 km thick layer with a 4% anisotropy [*Mainprice et al.*, 2000].

The Superior Craton contains 1079 pairs of measurements from 63 stations and shows large splitting times (1.12±0.31 s). The mean fast orientation is 47.8±17.5°. Fast orientations in the THO show three general patterns: NE in the north, W-E in the center, and SE in the south. The 414 measurements from 38 stations have a mean fast orientation of 67.8±32.0° and a mean splitting time of 0.93±0.30 s. The Wyoming Craton contains 314 measurements from 38 stations. The fast orientations, which are spatially inconsistent, have a mean of 65.0±41.0°. The mean splitting time for this area is 0.92±0.33 s. The Rio Grande rift contains 394 measurements from 31 stations. The mean splitting parameters are 82.0±26.8° and 0.98±0.32 s. The 1073 measurements from 115 stations in the Yavapai province have a mean fast orientation of 74.7±27.5° and a mean splitting time of 0.89±0.28 s. The mean splitting parameters of the 310 measurements from 26 stations in the MCR are 56.6±21.8° and 0.95±0.27 s, respectively. The 36 stations located in the Penokean province resulted in 312 measurements with mean splitting parameters 59.9± 30.8° and 0.90±0.29 s.

3.1. Relationship Between the Fast Orientations and the APM

We calculate the absolute differences between the APM and the observed fast orientations in the range of 0° to 90° for each of the 4210 ray-piercing points (including results of previous studies from Figure 1) at the depth of 200 km to illustrate the spatial variation of the fast orientations. The APM direction was determined using the model of *Gripp and Gordon* [2002] in a fixed hot spot frame. We obtained the absolute difference between the two directions and resampled the results in 1° × 1° overlaying blocks with a moving step of 0.05° (Figure 5). The results indicate that the fast orientations are about 30°–50° away from the APM in the THO and the Penokean orogeny and that the fast orientations in the Superior Craton generally correlate well with the APM direction. Fast orientations in the central Yavapai province vary spatially, leading to apparent deviations from the APM. Large deviations are observed in two areas: the Great Falls tectonic zone (centered

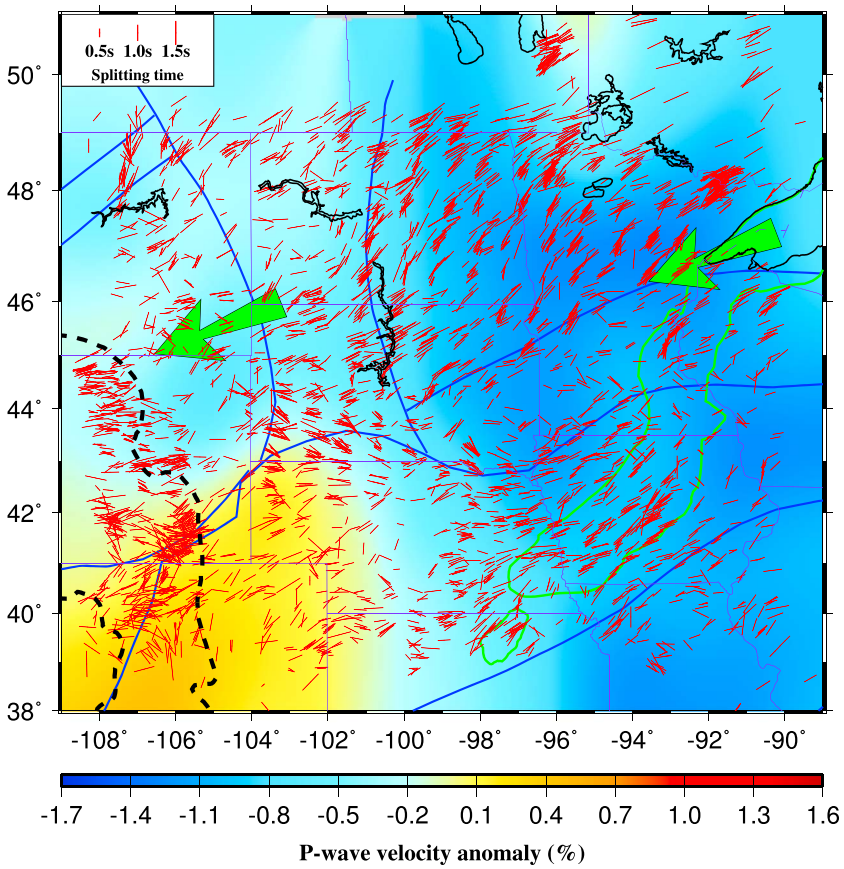

Figure 3. Shear wave splitting measurements plotted above 200 km ray-piercing points. The background image shows *P* wave velocity anomalies at the depth of 200 km [*Burdick et al.*, 2014]. The orientation of the red bars represents the fast orientation, and the length is proportional to the splitting time. The arrows indicate the APM direction.

at 109°W, 49°N) in which the fast orientations are mostly N-S and the Rio Grande rift (centered at 106°W, 38°N) in which the splitting parameters are spatially varying. For most other parts of the study area, the fast orientations and the APM are less than 30° apart (Figure 5).

3.2. Spatial Distribution of Splitting Times

The spatial distribution of splitting times (Figure 4) are investigated using the mean value of individual splitting times in overlapping 0.1° × 0.1° blocks with a moving step of 0.01°. The results (Figure 4) show that the splitting times decrease generally from north to south and the largest ones (>1.5 s) are located on the southwest part of the Superior Craton. Small splitting times (≤ 0.8 s) are located along the contact between the Yavapai and the Penokean provinces and in the central Yavapai province (Figure 4). The area covered by the MCR in the Yavapai province has larger splitting times than the surrounding areas. The THO and Wyoming Craton are characterized by splitting times of 0.7–1.0 s. Splitting times in the Rio Grande rift are about 1.0 s; this region generally shows the largest deviations between fast splitting orientations and APM direction.

4. Discussion

4.1. Spatial Distribution of Complex Anisotropy

Identification of complex anisotropy is essential for making reasonable interpretations of the SWS measurements and for understanding the *XKS* waveforms and the particle motion patterns, because complex anisotropy usually leads to an incomplete removal of *XKS* energy on the corrected transverse component [*Silver and Savage*, 1994; *Liu and Gao*, 2013]. The most common forms of complex anisotropy are characterized by systematic azimuthal variations of the splitting parameters [*Silver and Savage*, 1994]. On the other hand, for simple anisotropy, the apparent splitting parameters are invariant with the back azimuth.

We visually examine the observed splitting parameters for all of the 445 stations to identify the ones with systematic azimuthal variations. To quantitatively represent the spatial distribution of complex anisotropy,

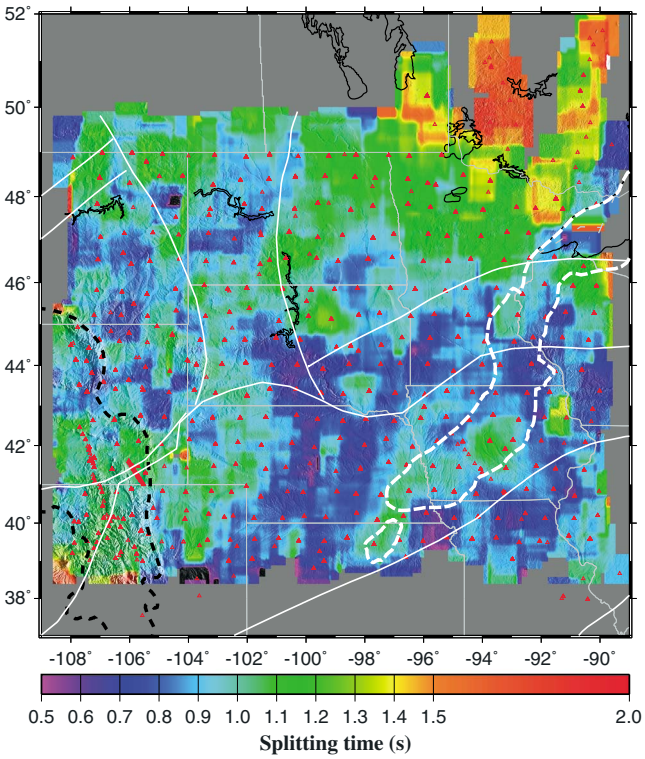

Figure 4. Spatial distribution of splitting times. Red triangles represent seismic stations used in the study.

we divide the stations into three types. For stations with no systematically varying splitting parameters, we assign a complex anisotropy index value of 0 to describe one-layer anisotropy (Figure 6a). We give an index value of 2 to stations with systematic azimuthal variations (Figures 6c and 6d), and a value of 1 to stations with poor azimuthal coverage (Figure 6b), at which the existence of complex anisotropy cannot be determined. We then spatially average the assigned index values using a cosine arch filter with a radius of 2° and moving step of 0.05°. The results (Figure 7) suggest that one-layer anisotropy is mostly located in the Superior craton (Area A) and the eastern part of the Yavapai province (Area B) in the study area. The area with complex anisotropy is mainly along the Yavapai-Penokean suture zone, on the Wyoming Craton, and along the Rio Grande rift (Figure 7, Area C).

In order to quantify the complex anisotropy using a two-layer model [*Silver and Savage*, 1994], we grid search for the two pairs of splitting parameters to fit the observed results in Area C. To obtain stable results, we combine nearby stations with similar patterns of azimuthal variation of the splitting parameters together and divide the area into 11 blocks. To reduce well-known ambiguities [*Gao and Liu*, 2009], we set the ϕ of the lower layer to be parallel to the APM direction and limit the splitting time of the lower layer, δt_1, in the range of 0.2 s to 1.5 s and search for the parameters of the upper layer. We also tested a number of other assumptions (e.g., fixing the ϕ of the upper layer to be parallel to the APM direction) and found that they could not produce a better fit to the observed data than the above assumption. Figure 8 shows the observed splitting parameters and the fitted results for the block in the vicinity of station J27Axx_TA. The resulting optimal splitting parameters for all the 11 blocks are shown in Figure 7. The fast orientations of the upper layer are mostly E-W, and for most of the blocks along the northern boundary of the Yavapai province, they are mostly consistent with the strikes of the boundary. The splitting times of the upper layer range from 0.35 s to 1.20 s, corresponding to a thickness of about 40–140 km for a layer with 4% anisotropy. The ϕ of the upper layer observed at the Wyoming Craton and the Rio Grande rift is NW-SE.

4.2. Testing the Hypothesis of Three-Layer Anisotropy

The three-layer anisotropic structure proposed by *Yuan and Romanowicz* [2010] from surface-wave inversion in our study area includes two layers in the lithosphere and one layer in the asthenosphere. The fast orientations of the top layer (from the surface to the depth of about 80 km), which has a very weak anisotropy of

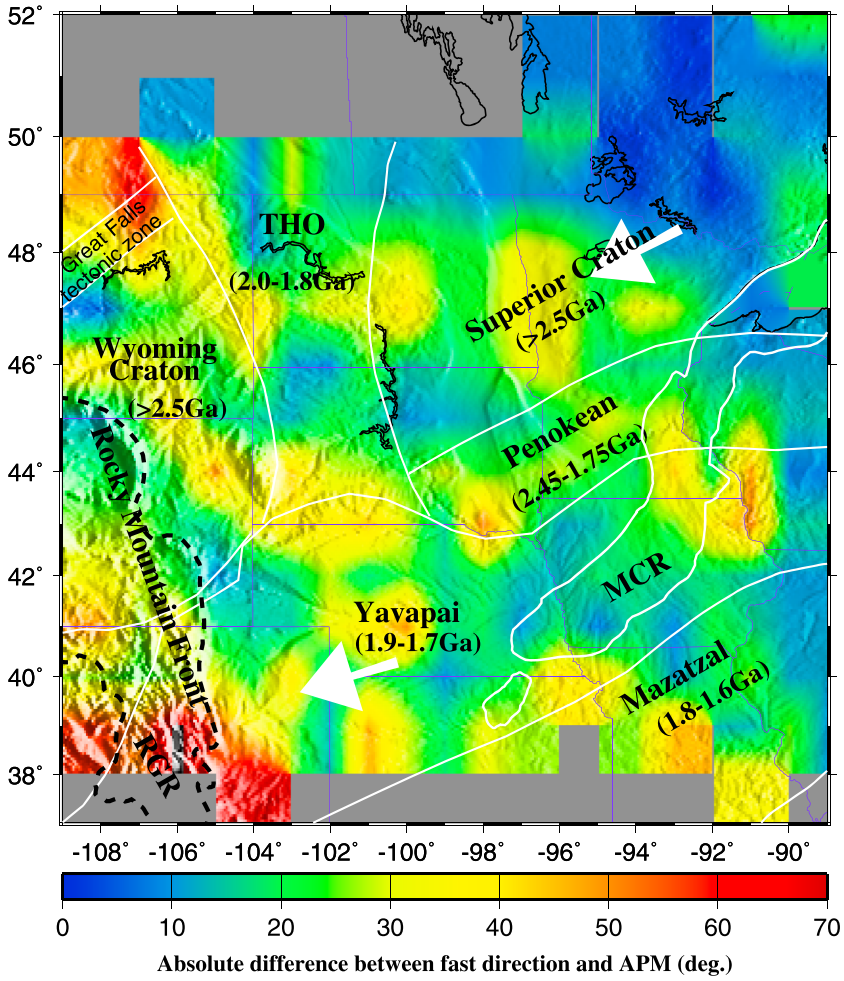

Figure 5. Absolute difference between the observed fast orientations and the APM direction (white arrows).

about 0.6–1.0%, are consistent with the geological trends. The splitting time of this layer can be up to about 0.2 s. The second layer has an approximately N-S fast orientation and a depth range of 80–200 km in the study area. The splitting time from this layer is about 0.6 s with a 2.0% anisotropy. The bottom layer, which resides in the asthenosphere, has an APM-parallel fast orientation and a strong anisotropy of 2.5%. A 1.0 s splitting time would be caused by this layer with a 200 km thickness.

To test the three-layer anisotropy model proposed by *Yuan and Romanowicz* [2010], we calculate theoretical splitting parameters based on the multiple-layer formula in *Silver and Savage* [1994]. The model has a lower layer with $\phi_1 = 70°$ and $\delta t_1 = 1.0$ s, a middle layer with $\phi_2 = 0°$ and $\delta t_2 = 0.7$ s, and an upper layer with $\phi_3 = 60°$ and $\delta t_3 = 0.3$ s. The results are plotted in Figures 9d and 9e. A clear pattern of $\pi/2$ periodicity is observed.

We verify the reliability of the three-layer curves by generating synthetic seismograms from the same three pairs of splitting parameters. The original shear wave before splitting has the form of $R(t) = A_0 \sin(2\pi ft)e^{-\alpha t}$ in which the amplitude $A_0 = 100$, frequency $f = 0.15$ Hz, and the decay factor $\alpha = 0.1$. The original transverse and radial components are calculated from 180 events with back azimuth ranging from 0 to 179° with an interval of 1°. Figure 9a shows the original transverse components. Figures 9d and 9e show the resulting apparent fast orientations and splitting times. The results from the synthetic test match very well with the theoretical curves.

We then compute theoretical apparent splitting parameters for a series of three-layer models with 57.0°–60.0° and 0.2–0.4 s for the top layer, −5.0°–5.0° and 0.6–0.8 s for the middle layer, and 70.0°–75.0° and 0.9–1.1 s for the bottom layer, with an interval of 1° for ϕ and 0.1 s for δt. Figure 8 shows some of the

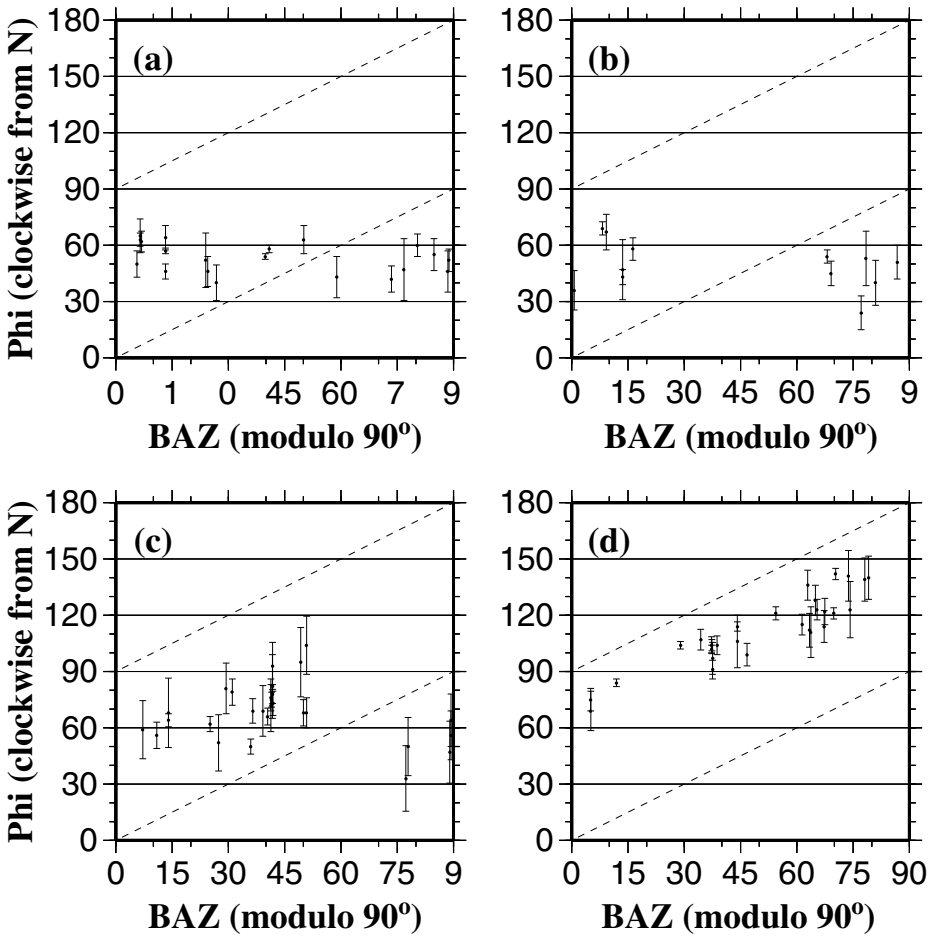

Figure 6. Azimuthal variation of observed fast orientations at four stations. (a) A27Axx_TA; (b) E31Axx_TA; (c) B28Axx_TA; and (d) J26Axx_TA.

representative resulting curves plotted on top of the observed splitting parameters for the block in the vicinity of station J27Axx_TA. A rather poor match is observed, suggesting that the three-layer model suggested by *Yuan and Romanowicz* [2010] is not consistent with the splitting parameters. The same comparison was made for the rest of the blocks with complex anisotropy, and none of them has a reasonable match between the observed and calculated splitting parameters. One possible reason for the discrepancy is that our study and the study of *Yuan and Romanowicz* [2010] used seismic waves in different frequency bands. With much longer period, the surface wave can characterize long-wavelength features, while the heterogeneities (smaller than the wavelength) in the anisotropic materials in the lithosphere cannot be detected. On the other side, *XKS* waves have shorter wavelengths and are sensitive to small heterogeneities so that the effect of anisotropy observed by *XKS* waves would be wiped out if the multiple layers and/or dipping axis of symmetry show strong heterogeneities. The above practice indicates that a three-layer model proposed by *Yuan and Romanowicz* [2010] cannot satisfactorily explain the SWS measurements, and the two-layer model presented in the previous section is adequate to represent the anisotropic structure in areas with complex anisotropy.

4.3. Anisotropy Depth Analysis

For Areas A and B which have simple anisotropy (Figure 7), we search the optimal depth of the observed anisotropy by computing a spatial variation factor [*Gao et al.*, 2010; *Liu and Gao*, 2011]. A detailed description of the procedure and an accompanying FORTRAN program can be found in *Gao and Liu* [2012]. The spatial variation factor, F_v, is computed for each depth from 0 to 400 km with an interval of 5 km [*Liu and Gao*, 2011]. Figure 10 shows the calculated F_v for the Superior Craton (Area A) and the eastern part of the Yavapai province (Area B). Beneath the Superior Craton, the depth estimate shows that the main contribution to

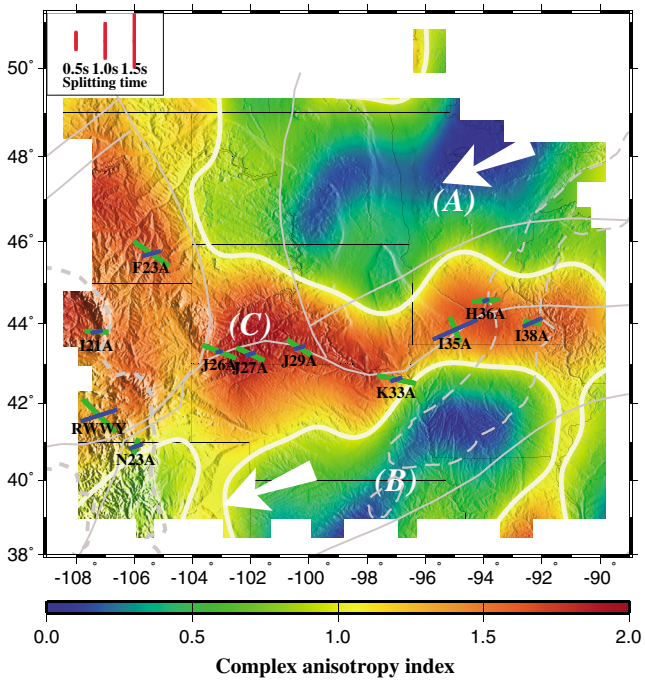

Figure 7. Spatial distribution of complex anisotropy index factors and results of grid searching for two-layer anisotropy parameters. The green and blue bars show the splitting parameters of the upper and lower layers, respectively. White arrows show the APM direction, and the white contour lines represent an index value of 1.0.

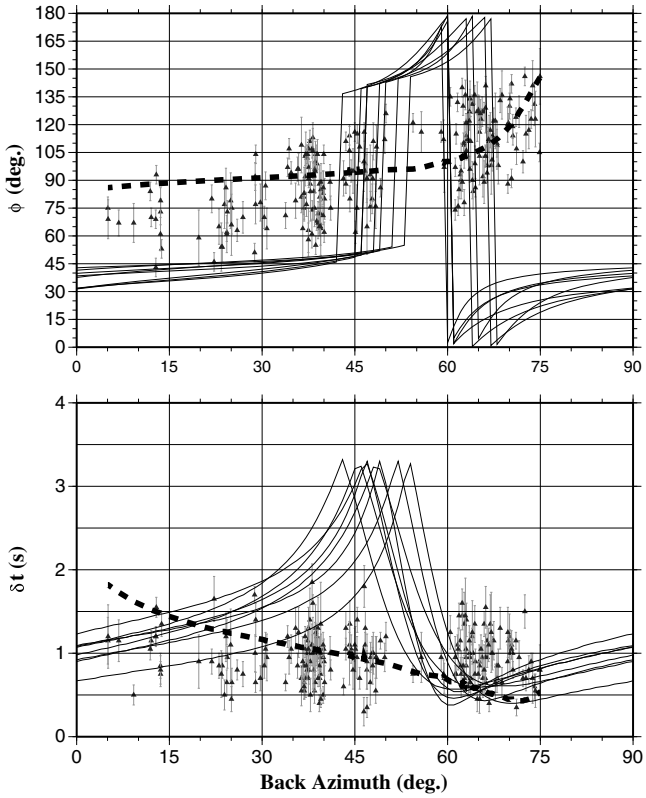

Figure 8. Azimuthal variations of observed splitting parameters at stations in the vicinity of J27Axx_TA. Data shown by the thick dashed lines were calculated using optimal parameters grid searched using a two-layer model, in which ϕ_1=70.0°, δt_1=0.95 s for the lower layer, and ϕ_2=-61.0°, δt_2=0.45 s for the upper layer. The thin solid lines show results calculated based on the three-layer model of *Yuan and Romanowicz* [2010] described in the text.

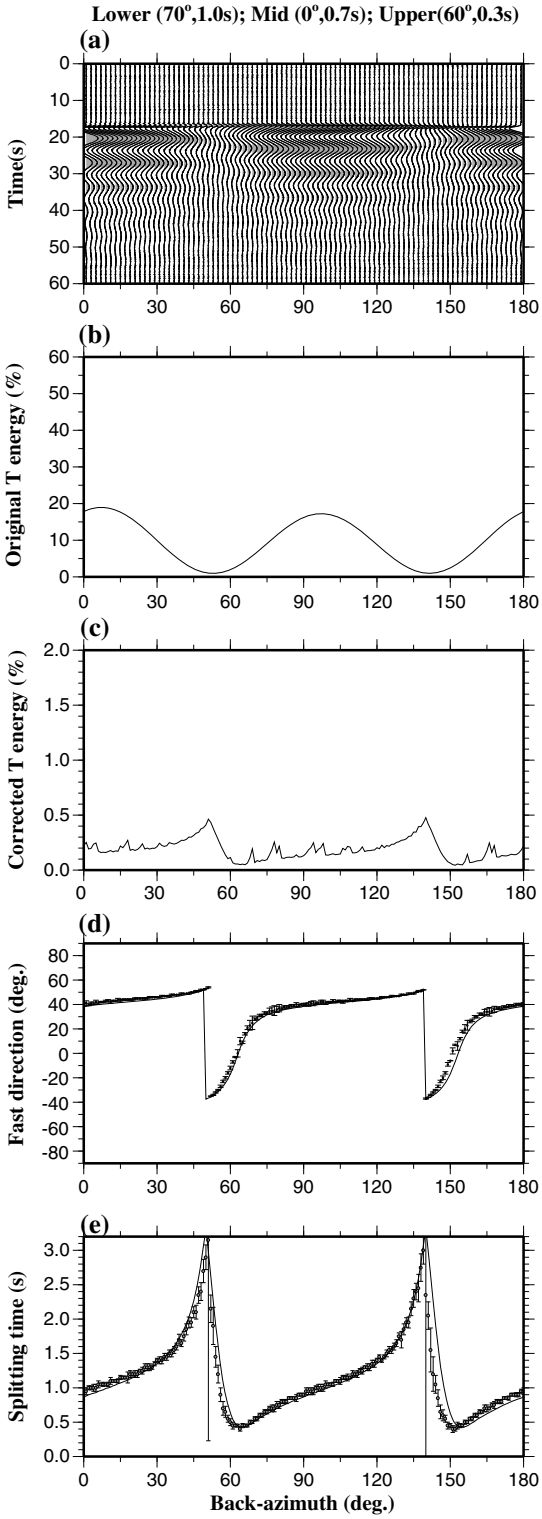

Figure 9. Synthetic seismograms and associated splitting parameters of a three-layer model. (a) Original transverse components; (b) energy on the original transverse components displayed as a percentage of that of the presplitting shear wave; (c) same as Figure 9b but for the corrected transverse components; (d) resulting apparent fast orientations; (e) resulting apparent splitting times. The black solid lines in Figures 9d and 9e are theoretical three-layer splitting parameters based on *Silver and Savage* [1994].

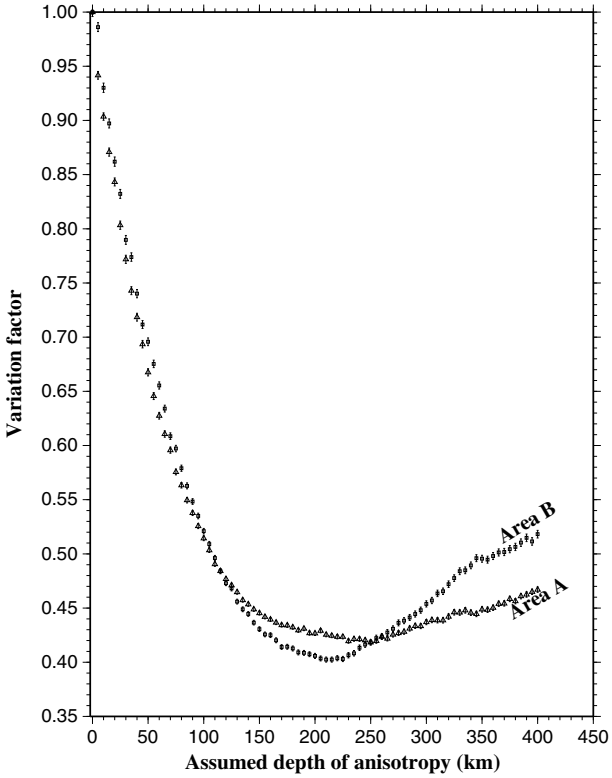

Figure 10. Anisotropy depth analysis for Areas A and B (Figure 7), estimated using the approach of *Gao and Liu* [2012].

the observed anisotropy comes from a depth of about 230–250 km, which is consistent with the depth of the lithosphere suggested by previous seismic tomography studies. *van der Lee and Frederiksen* [2005] and *Bedle and van der Lee* [2009] showed that the lithosphere thickness of the Superior Craton was 200–250 km, and *Darbyshire et al.* [2007] and *Darbyshire and Lebedev* [2009] inferred from Rayleigh wave phase velocity inversion that in our study area, the Superior province had a lithospheric thickness of approximately 140–200 km. Beneath the eastern Yavapai province, the resulting depth ranges from 200 to 230 km which is also consistent with previous estimates [*Yuan and Romanowicz*, 2010]. Such agreements suggest that the observed anisotropy mostly originates from the upper asthenosphere, a conclusion that is similar to the southern Great Plains [*Refayee et al.*, 2013].

4.4. Possible Lithospheric Contributions to Observed Anisotropy

Previous studies argued that much of the detected anisotropy beneath the study area had a lithospheric origin based on a limited number of SWS measurements [e.g., *Silver and Kaneshima*, 1993; *Frederiksen et al.*, 2013b]. As discussed below, although it is difficult to distinguish the contribution from the lithosphere and asthenosphere in areas where the APM is parallel to the Proterozoic sutures, several pieces of evidence suggest that collisional orogenies associated with the suture zones did not create significant vertically coherent deformation in the lithosphere, perhaps with the exception of the Superior Craton in the study area.

1. Small splitting times are observed along the suture zones. The maximum compressional strain in the study area is expected to be found along the suture zones, and consequently, large splitting times should be observed in the vicinity of the suture zones if the anisotropy is generated by compression. However, such a correlation is not observed at most of the suture zones (Figure 4). On the contrary, small splitting times are observed in the vicinity of the Yavapai-Penokean, the Yavapai-Mazatzal, and the THO-Penokean sutures.
2. With the exception of the Superior Craton, large splitting times are not positively correlated with lithospheric thickness revealed by seismic tomography [e.g., *Darbyshire et al.*, 2007; *Darbyshire and Lebedev*, 2009; *Burdick et al.*, 2014]. The largest splitting times in the study area (up to 1.7 s) are found in the Superior Craton, which has the greatest lithospheric thickness in the study area [*van der Lee and Frederiksen*, 2005; *Bedle and van der Lee*, 2009]. The similarity between the direction of the APM and the dominant

orientation of lithospheric structures in the Superior Craton makes it impossible to separate the contributions of fabrics in the lithosphere and the asthenosphere. Thus, the contributions from the lithosphere in this area cannot be quantified using SWS alone. Surface wave anisotropy studies [e.g., *Yuan and Romanowicz*, 2010] revealed an equivalent splitting time of about 1.0 s in the lithosphere, suggesting significant lithospheric contributions to the observed large splitting times in the Superior Craton.

3. The observed fast orientations are not parallel to some of the terrane boundaries. For instance, the majority of the fast orientations observed in the THO and the MCR are not consistent with their strikes. A pure-shear rifting mechanism, where both sides of the rift are pulled apart evenly [*Wilson et al.*, 2005], would cause a series of parallel fast orientations parallel to the dikes if the anisotropy is lithospheric [*Gao et al.*, 1997; 2010]. This parallelism is not observed.
4. Results of anisotropy depth analysis do not support a lithospheric origin. Results of the depth estimates using spatial coherency of SWS parameters (Figure 10) suggest that the depth of the anisotropy source is in the range of 220–250 km. These values are consistent with the thickness of the lithosphere beneath the area from various seismic tomography studies [*van der Lee and Nolet*, 1997; *Darbyshire and Lebedev*, 2009; *Bedle and van der Lee*, 2009 *Yuan and Romanowicz*, 2010; *Burdick et al.*, 2012, 2014]. Such agreements suggest that the observed anisotropy mostly originates from the base of the lithosphere and/or the top of the asthenosphere, where the maximum shear strain is expected.

4.5. An Asthenospheric Origin Model

For the majority of the study area, the lack of significant lithospheric contribution and the results of depth estimates (Figure 10) discussed above indicate that most of the observed anisotropy has an asthenospheric origin. A certain degree of coupling caused by the difference in viscosity between the lithosphere and the asthenosphere would generate an APM-parallel anisotropy in the upper asthenosphere [*Marone and Romanowicz*, 2007; *Refayee et al.*, 2013]. A smaller viscosity difference would lead to a larger degree of coupling [*Doglioni et al.*, 2011], causing a larger splitting time.

Studies on geodynamic modeling and seismic tomography [*Becker et al.*, 2006; *Forte et al.*, 2007] indicated a dominantly northeastward directed asthenospheric flow (relative to the lithosphere) beneath most part of the study area. A mantle flow system proposed by *Refayee et al.* [2013] provides a viable explanation for the measurements observed on the southwestern edge of the North American continent. Here, we combine our results with those by *Refayee et al.* [2013] and propose a mantle flow model (Figure 11) that can explain most of our observations.

In the model, the central United States is divided into five zones with different dominant anisotropy-forming mechanisms. This model suggests that partial coupling between the lithosphere and the underlying asthenosphere is responsible for the APM-parallel simple anisotropy observed in Zones I and V (Figure 11). The larger-than-normal splitting times beneath the Superior Craton (Zone II) probably imply a greater degree of coupling between the lithosphere and the asthenosphere, as the result of a reduced viscosity contrast between the thick lithosphere and the asthenosphere. Alternatively, they may reflect significant lithospheric contributions.

The continental root moving southwestward (relative to the asthenosphere) deflects the asthenospheric flow along its western edge (Figure 11, the N-S section of Zone IV), leading to N-S fast orientations. The flow system changes its direction and turns eastward around the southwest corner of the North American continent. The southwestward movement of the North American continent also induces a flow system along a lithospheric channel (Zone III in Figure 11), which is a zone of thinned lithosphere, approximately beneath the northern boundary of the Yavapai province. The existence of the channel is suggested by surface wave tomography using USArray data [*Frederiksen et al.*, 2013a]. We propose that simple shear between the flow system in the channel and the lithosphere is responsible for the anisotropy of the top layer observed in Zone III, and partial coupling between the flow in the channel and the underlying asthenosphere leads to the APM-parallel anisotropy in the bottom layer.

A joint point of the channeled and deflected flow systems may exist beneath the northern Rio Grande rift (Figure 11), approximately at (106.5°W, 40.0°N). The mantle flow separates from this point, with one branch traveling southward and another moving northeastward along the lithospheric channel. The existence of the joint point is supported by the spatially rapid-varying splitting parameters near the proposed location.

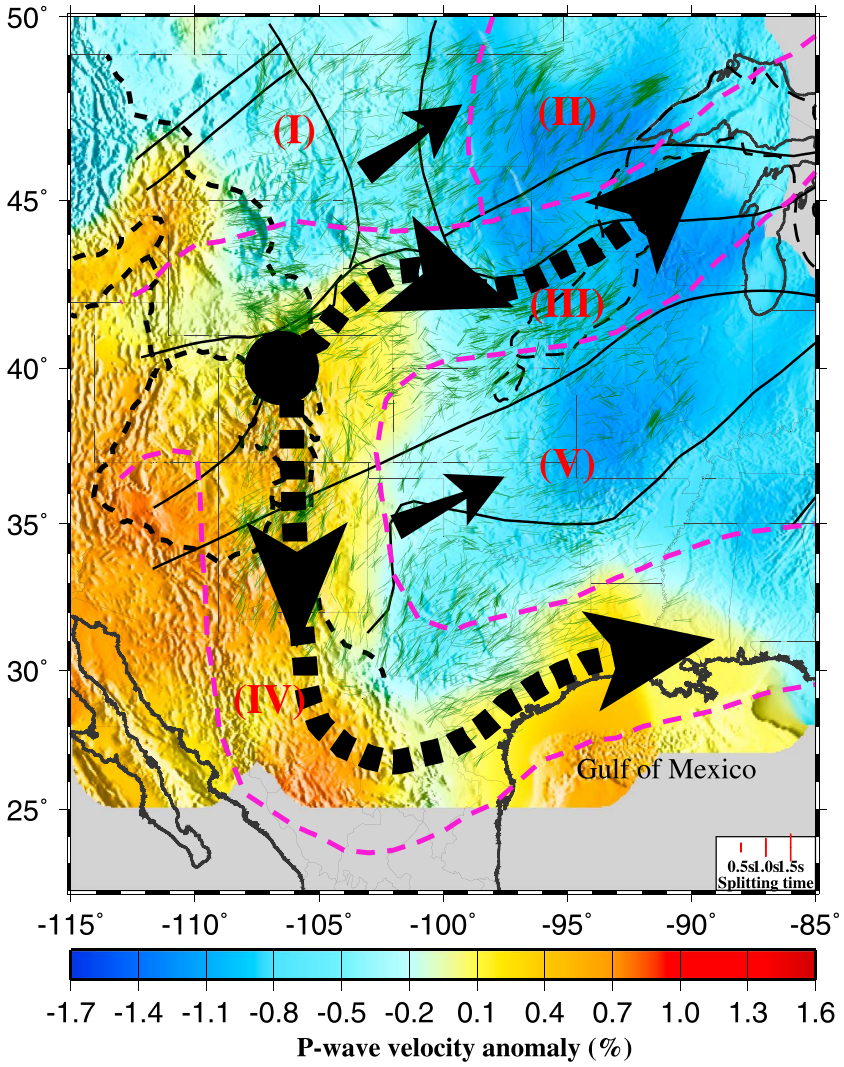

Figure 11. Schematic diagram showing direction of flow lines in the asthenosphere relative to the lithosphere with a background of *P* wave velocity anomalies at the depth of 200 km [*Burdick et al.*, 2012]. The short solid arrows indicate shear strain in the asthenosphere beneath the continent associated with APM, and the thick dashed arrows represent flow deflected by the bottom of the North American lithosphere and flow in the lithospheric channel. The thin bars represent individual shear wave splitting measurements, and the black dot is the joint point of the flow systems. The purple dash lines isolate five zones with different dominant anisotropy-forming mechanisms.

5. Conclusions

Over 4000 pairs of shear wave splitting parameters with unprecedented spatial resolution are observed on the northern Great Plains of North America. Although lithospheric contributions to the observed anisotropy can not be completely ruled out especially beneath the Superior province, depth estimates using spatial coherency of the splitting parameters and the dominantly APM-parallel fast orientations imply that coupling between the lithosphere and the asthenosphere is the most likely cause of the observed anisotropy. Along the northern boundary of the Yavapai province, beneath which a zone of thinned lithosphere is revealed by seismic tomography, a double-layer anisotropy model can satisfactorily explain the azimuthal dependence of the splitting parameters. The top layer is most likely associated with simple shear between the base of the lithosphere and mantle flow in the lithospheric channel, and anisotropy in the lower layer could originate from the differential movement between the channel flow and the underlying APM-parallel flow, which is also responsible for the APM-parallel anisotropy observed in areas with simple anisotropy. We propose that the edge-parallel flow system is driven by the southwestward movement of the bottom of the continental lithosphere, which gradually deepens toward the interior of the North American continent, as revealed

by seismic tomography studies [*van der Lee and Frederiksen*, 2005; *Darbyshire et al.*, 2007; *Bedle and van der Lee*, 2009; *Darbyshire and Lebedev*, 2009; *Burdick et al.*, 2014]. Such movement deflects mantle flow and leads to N-S and E-W oriented fast orientations observed along the western and southern edges of the North American continent, respectively. Results from this study, when combined with those from previous shear wave splitting and other geophysical modeling and observational investigations, support the notion that shear strain associated with partial coupling between the lithosphere and the asthenosphere contributes to the bulk of the observed anisotropy on plates with a significant differential movement relative to the underlying asthenosphere.

Acknowledgments

Data used in the study were obtained from the IRIS Data Management System. We are grateful to the Associate Editor and two anonymous reviewers for their very thoughtful constructive comments and suggestions. This study was supported by the U.S. National Science Foundation under grant EAR-0952064 to S.G. and K.L. and the University of Missouri Research Board.

References

Balch, R. S., H. E. Hartse, A. R. Sanford, and K. W. Lin (1997), A new map of the geographic extent of the Socorro mid-crustal magma body, *Bull. Seismol. Soc. Am.*, *87*, 174–182.

Baldridge, W. S., F. V. Perry, D. T. Vaniman, L. D. Nealey, B. D. Leavy, A. W. Laughlin, P. R. Kyle, Y. Bartov, G. Steintz, and E. S. Gladney (1991), Middle to late Cenozoic magmatism of the southeastern Colorado Plateau and central Rio Grande rift (New Mexico and Arizona, USA): A model for continental rifting, *Tectonophysics*, *197*, 327–354.

Barruol, G., G. Helffrich, and A. Vauchez (1997a), Shear wave splitting around the northern Atlantic, frozen Pangaean lithospheric anisotropy, *Tectonophysics*, *279*(1-4), 135–148.

Barruol, G., P. G. Silver, and A. Vauchez (1997b), Seismic anisotropy in the eastern United States: Deep structure of complex continental plate, *J. Geophys. Res.*, *102*, 8329–8348, doi:10.1029/96JB03800.

Becker, T. W., V. Schulte-Pelkum, D. K. Blackman, J. B. Kellogg, and R. J. O'Connell (2006), Mantle flow under the Western United States from shear wave splitting, *Earth Planet. Sci. Lett.*, *247*, 235–251.

Bedle, H., and S. van der Lee (2009), S velocity variations beneath North America, *J. Geophys. Res.*, *114*, B07308, doi:10.1029/2008JB005949.

Bormann, P., G. Grunthal, R. Kind, and H. Montag (1996), Upper mantle anisotropy beneath Central Europe from SKS wave splitting: Effects of absolute plate motion and lithosphere-asthenosphere boundary topography?, *J. Geodyn.*, *22*, 11–32.

Burdick, S., R. D. Van Der Hilst, F. L. Vernon, V. Martynov, T. Cox, J. Eakins, G. H. Karasu, J. Tylell, L. Astiz, and G. L. Pavlis (2012), Model update March 2011: Upper mantle heterogeneity beneath North America from traveltime tomography with global and USArray transportable array data, *Seismol. Res. Lett.*, *83*, 23–28, doi:10.1785/gssrl.83.1.23.

Burdick, S., R. D. Van Der Hilst, F. L. Vernon, V. Martynov, T. Cox, J. Eakins, G. H. Karasu, J. Tylell, L. Astiz, and G. L. Pavlis (2014), Model update January 2013: Upper mantle heterogeneity beneath North America from travel-time tomography with global and USArray transportable array data, *Seismol. Res. Lett.*, *85*, 77–81, doi:10.1785/0220130098.

Conrad, C. P., and M. D. Behn (2010), Constraints on lithosphere net rotation and asthenospheric viscosity from global mantle flow models and seismic anisotropy, *Geochem. Geophys. Geosyst.*, *11*, Q05W05, doi:10.1029/2009GC002970.

Coward, M. P., R. W. H. Butler, M. A. Khan, and R. J. Knipe (1987), The tectonic history of Kohistan and its implications for Himalayan structure, *J. Geol. Soc., London*, *144*, 377–391.

Darbyshire, F. A., D. W. Eaton, A. W. Frederiksen, and L. Ertolahti (2007), New insights into the lithosphere beneath the Superior Province from Rayleigh wave dispersion and receiver function analysis, *Geophys. J. Int.*, *169*, 1043–1068, doi:10.1111/j.1365-246X.2006.03259.x.

Darbyshire, F. A., and S. Lebedev (2009), Rayleigh wave phase-velocity heterogeneity and multilayered azimuthal anisotropy of the Superior Craton, Ontario, *Geophys. J. Int.*, *176*, 215–234.

Davidson, A. (1995), A review of the Grenville orogen in its North American type area, *J. Austra. Geol. Geophys.*, *16*, 3–24.

Doglioni, C., A. Ismail-Zadeh, G. Panza, and F. Riguzzi (2011), Lithosphere-asthenosphere viscosity contrast and decoupling, *Phys. Earth Planet. Inter.*, *189*, 1–8.

Forte, A. M., J. X. Mitrovica, R. Moucha, N. A. Simmons, and S. P. Grand (2007), Descent of the ancient Farallon slab drives localized mantle flow below the New Madrid seismic zone, *Geophys. Res. Lett.*, *34*, L04308, doi:10.1029/2006GL027895.

Fouch, M. J., and S. Rondenay (2006), Seismic anisotropy beneath stable continental interiors, *Phys. Earth Planet. Inter.*, *158*, 292–320, doi:10.1016/j.pepi.2006.01.022.

Frederiksen, A. W., T. Bollmann, F. Darbyshire, and S. van der Lee (2013a), Modification of continental lithosphere by tectonic processes: A tomographic image of central North America, *J. Geophys. Res. Solid Earth*, *18*, 1051–1066, doi:10.1002/jgrb.50060.

Frederiksen, A. W., I. Deniset, O. Ola, and D. Toni (2013b), Lithospheric fabric variations in central North America: Influence of rifting and Archean tectonic styles, *Geophys. Res. Lett.*, *40*, 4583–4587, doi:10.1002/grl.50879.

Frederiksen, A. W., S. K. Miong, F. A. Darbyshire, D. W. Eaton, S. Rondenay, and S. Sol (2007), Lithospheric variations across the superior Province, Ontario, Canada: Evidence from tomography and shear-wave splitting, *J. Geophys. Res.*, *112*, B07318, doi:10.1029/2006JB004861.

Gao, S. S., P. M. Davis, K. H. Liu, P. D. Slack, A. W. Rigor, Y. A. Zorin, V. V. Mordvinova, V. M. Kozhevnikov, and N. A. Logatchev (1997), *SKS* splitting beneath continental rift zones, *J. Geophys. Res.*, *102*, 22,781–22,797.

Gao, S. S., and K. H. Liu (2009), Significant seismic anisotropy beneath the southern Lhasa Terrane, Tibetan Plateau, *Geochem. Geophys. Geosyst.*, *10*, Q02008, doi:10.1029/2008GC002227.

Gao, S. S., and K. H. Liu (2012), AnisDep: A FORTRAN program for the estimation of the depth of anisotropy using spatial coherency of shear-wave splitting parameters, *Comput. Geosci.*, *49*, 330–333, doi:10.1016/j.cageo.2012.01.020.

Gao, S. S., K. H. Liu, and M. G. Abdelsalam (2010), Seismic anisotropy beneath the Afar Depression and adjacent areas: Implications for mantle flow, *J. Geophys. Res.*, *115*, B12330, doi:10.1029/2009JB007141.

Grand, S. P., and D. V. Helmberger (1984), Upper mantle shear structure beneath the northwest Atlantic Ocean, *J. Geophys. Res.*, *89*, 11,465–11,475.

Gripp, A. E., and R. G. Gordon (2002), Young tracks of hotspots and current plate velocities, *Geophys. J. Int.*, *150*, 321–361.

Hoffman, P. F. (1988), United plates of America, the birth of a craton: Early Proterozoic assembly and growth in Laurentia, *Annu. Rev. Earth Planet. Sci.*, *16*, 543–603.

Hoffman, P. F. (1989), Precambrian geology and tectonic history of North America, in *The Geology of North America—An Overview*, edited by A. W. Bally and A. R. Palmer, pp. 447–512, Geol. Soc. Amer., Boulder, Colo.

Holm, D. (1999), A geodynamic model for Paleoproterozoic post-tectonic magma genesis in the southern Trans-Hudson and Penokean orogens, *Rocky Mt Geol.*, *34*, 183–194, doi:10.2113/34.2.183.

Huang, Z., L. Wang, D. Zhao, N. Mi, and M. Xu (2011), Seismic anisotropy and mantle dynamics beneath China, *Earth Planet. Sci. Lett.*, *306*, 105–117.
Karlstrom, K. E., and S. A. Bowring (1988), Early Proterozoic assembly of tectono-stratigraphic terranes in southwestern North America, *J. Geol.*, *96*, 561–576.
Kay, I., S. Sol, J.-M. Kendall, C. Thomson, D. White, I. Asudeh, B. Roberts, and D. Francis (1999), Shear wave splitting observations in the Archean Craton of Western Superior, *Geophys. Res. Lett.*, *26*, 2669–2672.
Kendall, J.-M., G. W. Stuart, C. Ebinger, I. D. Bastow, and D. Keir (2005), Magma-assisted rifting in Ethiopia, *Nature*, *433*, 146–148.
Kreemer, C. (2009), Absolute plate motions constrained by shear wave splitting orientations with implications for hotspot motions and mantle flow, *J. Geophys. Res.*, *114*, B10405, doi:10.1029/2009JB006416.
Lawton, T. F., and N. J. McMillan (1999), Arc abandonment as a cause for passive continental rifting: Comparison of the Jurassic Mexican Borderland rift and the Cenozoic Rio Grande rift, *Geology*, *27*, 779–782.
Li, Y., Q. Wu, F. Zhang, Q. Feng, and R. Zhang (2011), Seismic anisotropy of the northeastern Tibetan Plateau from shear wave splitting analysis, *Earth Planet. Sci. Lett.*, *304*, 147–157, doi:10.1016/j.epsl.2011.01.026.
Liu, K. H. (2009), NA-SWS-1.1: A uniform database of teleseismic shear-wave splitting measurements for North America, *Geochem. Geophys. Geosyst.*, *10*, Q05011, doi:10.1029/2009GC002440.
Liu, K. H., and S. S. Gao (2011), Estimation of the depth of anisotropy using spatial coherency of shear-wave splitting parameters, *Bull. Seismol. Soc. Am.*, *101*, 2153–2161.
Liu, K. H., and S. S. Gao (2013), Making reliable shear-wave splitting measurements, *Bull. Seismol. Soc. Am.*, *103*, 2680–2693, doi:10.1785/0120120355.
Liu, K. H., S. S. Gao, Y. Gao, and J. Wu (2008), Shear wave splitting and mantle flow associated with the deflected slab beneath northeast Asia, *J. Geophys. Res.*, *113*, B01305, doi:10.1029/2007JB005178.
Long, M. D., and P. G. Silver (2009), Shear wave splitting anisotropy: Measurements, interpretation, and new directions, *Surv. Geophys.*, *30*, 407–461.
Mainprice, D., G. Barruol, and W. Ben Ismail (2000), The seismic anisotropy of the Earth's mantle: From single crystal to polycrystal, in *Earth's Deep Interior: Mineral Physics and Tomography From the Atomic to the Global Scale*, edited by S. I. Karato, pp. 237–264, AGU, Washington, D. C.
Marone, F., and B. Romanowicz (2007), The depth distribution of azimuthal anisotropy in the continental upper mantle, *Nature*, *447*, 198–201.
Maupin, V., E. J. Garnero, T. Lay, and M. J. Fouch (2005), Azimuthal anisotropy in the D layer beneath the Caribbean, *J. Geophys. Res.*, *110*, B08301, doi:10.1029/2004JB003506.
McMillan, J., A. P. Dickin, and D. Haag (2000), Evolution of magma source regions in the Rio Grande rift, southern New Mexico, *Geol. Soc. Am. Bull.*, *112*, 1582–1593.
Morgan, P., W. R. Seager, and M. P. Golombek (1986), Cenozoic thermal mechanical and tectonic evolution of the Rio Grande rift, *J. Geophys. Res.*, *91*, 6262–6276.
Mosher, S. (1998), Tectonic evolution of the southern Laurentian Grenville orogenies belt, *Geol. Soc. Am. Bull.*, *110*, 1357–1375.
Refayee, H. A., B. B. Yang, K. H. Liu, and S. S. Gao (2013), Mantle flow and lithosphere-asthenosphere coupling beneath the southwestern edge of the North American craton: Constrains from shear-wave splitting measurements, *Earth Planet. Sci. Lett.*, doi:10.1016/j.epsl.2013.01.031i.
Sandvol, E., and J. Ni (1994), Mapping seismic azimuthal anisotropy in the United States from LRSM short period data, *Eos Trans. AGU*, *75*, 481.
Satsukawa, T., K. Michibayashi, E. Y. Anthony, R. J. Stern, S. S. Gao, and K. H. Liu (2011), Seismic anisotropy of the uppermost mantle beneath the Rio Grande rift: Evidence from Kilbourne Hole peridotite xenoliths, New Mexico, *Earth Planet. Sci. Lett.*, *311*, 172–181.
Savage, M. K. (1999), Seismic anisotropy and mantle deformation: What have we learned from shear wave splitting?, *Rev. Geophys.*, *37*, 65–106.
Savage, M. K., A. F. Sheehan, and A. Lerner-Lam (1996), Shear wave splitting across the Rocky Mountain Front, *Geophys. Res. Lett.*, *23*, 2267–2270.
Silver, P. G. (1996), Seismic anisotropy beneath the continents: Probing the depths of geology, *Annu. Rev. Earth Planet. Sci.*, *24*, 385–432.
Silver, P. G., and W. W. Chan (1991), Shear wave splitting and subcontinental mantle deformation, *J. Geophys. Res.*, *96*, 16,429–16,454.
Silver, P. G., and W. E. Holt (2002), The mantle flow field beneath western North America, *Science*, *295*, 1054–1057, doi:10.1126/science.1066878.
Silver, P. G., and S. Kaneshima (1993), Constraints on mantle anisotropy beneath Precambrian North America from a transportable teleseismic experiment, *Geophys. Res. Lett.*, *20*, 1127–1130.
Silver, P. G., and M. Savage (1994), The interpretation of shear-wave splitting parameters in the presence of two anisotropic layers, *Geophys. J. Int.*, *119*, 949–963, doi:10.1111/j.1365-246X.1994.tb04027.x.
Tommasi, A., A. Vauchez, and R. Russo (1996), Seismic anisotropy in oceanic basins: Resistive drag of the sublithospheric mantle?, *Geophys. Res. Lett.*, *23*, 2991–2994.
van der Lee, S., and A. Frederiksen (2005), Surface wave tomography applied to the North American upper mantle, in *Seismic Data Analysis and Imaging With Global and Local Arrays*, vol. 157, edited by G. Nolet and A. Levander, pp. 67–80, Amer. Geophys. Union Monograph, Washington, D. C.
van der Lee, S., and G. Nolet (1997), Upper mantle S velocity structure of North America, *J. Geophys. Res.*, *102*, 22,815–22,838, doi:10.1029/97JB01168.
Vinnik, L. P., L. J. Makeyeva, A. Milev, and A. Y. Usenko (1992), Global patterns of azimuthal anisotropy and deformations in the continental mantle, *Geophys. J. Int.*, *111*, 433–447.
Whitmeyer, S. J., and K. E. Karlstrom (2007), Tectonic model for the Proterozoic growth of North America, *Geosphere*, *3*, 220–259.
Wilson, D., R. Aster, W. West, J. Ni, S. Grand, W. Gao, W. S. Baldridge, and P. Patel (2005), Lithospheric structure of the Rio Grande rift, *Nature*, *433*, 851–855.
Yuan, H., and B. Romanowicz (2010), Lithospheric layering in the North American craton, *Nature*, *466*, 1063–1069.
Zhao, G. C., P. A. Cawood, S. A. Wilde, and M. Sun (2002), Review of global 2.1-1.8 Ga orogens: Implications for a pre-Rodinia supercontinent, *Earth Sci. Rev.*, *59*, 125–162.